UCLA
UCLA Previously Published Works

Title

Volume Averaging Theory (VAT) based modeling and closure evaluation for fin-and-tube heat exchangers

Permalink

https://escholarship.org/uc/item/3pr0647r

Journal

Heat and Mass Transfer, 48(10)

ISSN

0947-7411 1432-1181

Authors

Zhou, Feng
Catton, Ivan

Publication Date

2012-06-14

DOI

10.1007/s00231-012-1025-7

Peer reviewed

eScholarship.org Powered by the California Digital Library
University of California

Heat Mass Transfer (2012) 48:1813–1823
DOI 10.1007/s00231-012-1025-7

ORIGINAL

Volume Averaging Theory (VAT) based modeling and closure evaluation for fin-and-tube heat exchangers

Feng Zhou · Ivan Catton

Received: 9 January 2012 / Accepted: 23 May 2012 / Published online: 14 June 2012
© Springer-Verlag 2012

Abstract A fin-and-tube heat exchanger was modeled based on Volume Averaging Theory (VAT) in such a way that the details of the original structure was replaced by their averaged counterparts, so that the VAT based governing equations can be efficiently solved for a wide range of parameters. To complete the VAT based model, proper closure is needed, which is related to a local friction factor and a heat transfer coefficient of a Representative Elementary Volume (REV). The terms in the closure expressions are complex and sometimes relating experimental data to the closure terms is difficult. In this work we use CFD to evaluate the rigorously derived closure terms over one of the selected REVs. The objective is to show how heat exchangers can be modeled as a porous media and how CFD can be used in place of a detailed, often formidable, experimental effort to obtain closure for the model.

Abbreviations

A	Area (m^2)
A_f	Fin surface area (m^2)
A_o	Total surface area (m^2)
A_w	Wetted surface (m^2)
A_{wp}	The cross flow projected area (m^2)
c_p	Specific heat (J/(kg·K))
D_i	Inner diameter of the tube (m)
D_o	Outer diameter of the tube (m)
D_c	Fin collar outside diameter, $D_c = D_o + 2\delta_f$ (m)
D_h	Porous media hydraulic diameter (m)
d_p	Diameter of the spherical particles (m)
F_1, F_2	Blending function
F_p	Fin pitch (m)
f	Friction factor
h	Heat transfer coefficient (W/(m^2·K))
k	Turbulence kinetic energy per unit mass
k_f	Thermal conductivity of the fluid (W/(m·K))
k_s	Thermal conductivity of the solid (W/(m·K))
k_T	Turbulent heat conductivity (W/(m·K))
m	$\sqrt{(2h)/(\lambda_f \delta_f)}$, parameter
$\dot{m}$	Mass flow rate (kg/s)
$\langle m \rangle$	Average porosity
N	The number of tube rows
Nu	Nusselt number
P_k	Shear production of turbulence
Pr	Prandtl number
Pr_T	Turbulent Prandtl number
P_t	Transverse tube pitch (m)
P_l	Longitudinal tube pitch (m)
p	Pressure (Pa)
Re_{D_c}	Reynolds number based on fin collar outside diameter and maximum velocity, $Re_{D_c} = u_{max} D_c / v$
Re_{D_h}	Reynolds number based on hydraulic diameter and average velocity, $Re_{D_h} = \bar{\bar{u}} D_h / v$
R_{eq}	Equivalent radius for circular fin (m)
r	Radius of tube, including collar thickness (m)
S	An invariant measure of the strain rate
S_w	Specific surface of a porous media, $S_w = \partial S_w / \Delta\Omega$ (1/m)
S_{wp}	The cross flow projected area per volume (1/m)
T	Fluid temperature (K)
T_s	Solid temperature (K)
u	x direction velocity term (m/s)
w	z direction velocity term (m/s)

F. Zhou (✉) · I. Catton
Department of Mechanical and Aerospace Engineering, University of California, Los Angeles, CA, USA
e-mail: zhoufeng@ucla.edu

I. Catton
e-mail: catton@ucla.edu

X_L $\sqrt{(P_t/2)^2+P_l^2}\Big/2$, geometric parameter (m)

X_M $P_t/2$, geometric parameter (m)

Greek

α Turbulence model constant or scale attack angle

β, β^* Turbulence model constant

φ_1 Represent any constant in the original k-ω model ($\sigma_{k1}, \ldots$)

φ_2 Represent any constant in the transformed k-ε model ($\sigma_{k2}, \ldots$)

φ Represent the corresponding constant in the SST model ($\sigma_k, \ldots$)

δ_f Thickness of a fin (m)

μ Viscosity (Pa·s)

μ_T Turbulent eddy viscosity (Pa·s)

v Kinematic viscosity (m^2/s)

v_T Turbulent kinematic viscosity (m^2/s)

ρ Density (kg/m^3)

σ_ε k-ε turbulence model constant

σ_k Turbulence model constant for the k equation

σ_ω k-ω turbulence model constant

τ_{wL} Laminar shear stress (N/m^2)

τ_{wT} Turbulent shear stress (N/m^2)

$\Delta\Omega$ The volume of the REV (m^3)

ω Specific turbulence dissipation rate

Subscripts and superscripts

$\sim$ A value averaged over the representative volume

– An average of turbulent values

^ Fluctuation of a value

$\langle f \rangle_f$ Means the superficial average of the function f

f Fluid phase or fin surface

in Air-side inlet

out Air-side outlet

T Turbulent

s Solid phase

1 A value in the air side

2 A value in the water side

0 Evaluated at the wall or surface

b Evaluated at the bulk temperature

1 Introduction

A plane fin-and-tube heat exchanger (FTHX) consisting of tubes and plate fins with air as one of the fluids has many engineering applications, such as air conditioning systems, air heaters, waste and process heat recovery, radiators, etc. There are many variants relating to fin patterns of the fin-and-tube heat exchangers such as plane fins, wavy fins, louvered fins, slotted fins, offset strip fins, etc. Among them plane fin is still the most popular fin pattern due to its simplicity, durability, and versatility in application. A schematic diagram of a plane fin-and-tube heat exchanger is shown in Fig. 1a.

Extensive investigations on the performance of fin-and-tube heat exchangers have been done, either experimentally [1–8] or numerically [9–12]. Most of them [1–3, 5, 6, 8, 9, 11, 12] are investigations on the effect of geometric parameters, such as tube diameter, tube pitches, fin pitches, etc. on the flow and heat transfer characteristics of FTHXs or proposal of correlations for air-side heat transfer coefficient and friction factor [4, 7]. To find the optimum configurations for these kinds of heterogeneous hierarchical heat transfer devices, which require many parameters to describe their geometries, experiment or CFD simulation by itself is out of the question. In the case of a fin-and-tube heat exchanger, 15 parameters are required for its description: overall length, width and height, fin thickness, fin pitch, tube diameter, tube wall thickness, tube pitch in x and y directions, flow rates of fluid 1 and 2, initial temperatures of fluid 1, 2, material of construction and heat source.

If one wants to optimize such a heat transfer device, simple equations are the only answer but they need to be made more rigorous and must include conjugate effects. In this work, VAT, see [13–20], will be used to develop the needed simple equations allowing clear rigorous statements to be made that define how the friction factor and heat transfer coefficient are to be determined. By modeling FTHXs as porous media, specific geometry can be accounted for in such a way that the details of the original structure can be replaced by their averaged counterparts and the governing VAT equations can be solved for a wide range of design parameters. This 'porous media' model, which is a function only of porous media morphology, represented by porosity and specific surface area, and its closure, can easily be adapted to many different structures.

Closure theories for transport equations in heterogeneous media have been the primary measure of advancement and for measuring success in research on transport in porous media. Obtaining closure for the VAT based governing equation set is the most difficult aspect of using VAT to model and optimize a heat transfer device. The porosity and specific surface area are geometrically defined terms. The closure terms, which are related to a local friction factor and a heat transfer coefficient, can be obtained in two ways. The first is to rescale the available experimental data reported for fully developed flow, using the 'porous media' length scale suggested by VAT [16–18, 20]. Zhou et al. [21] and Geb et al. [22] demonstrated how the experimental data and correlations available in public literature could be collected and used to obtain the closure by rescaling these data using VAT suggested length scale. However, sometimes, obtaining closure by relating experimental data to the closure terms is difficult. The difficulty

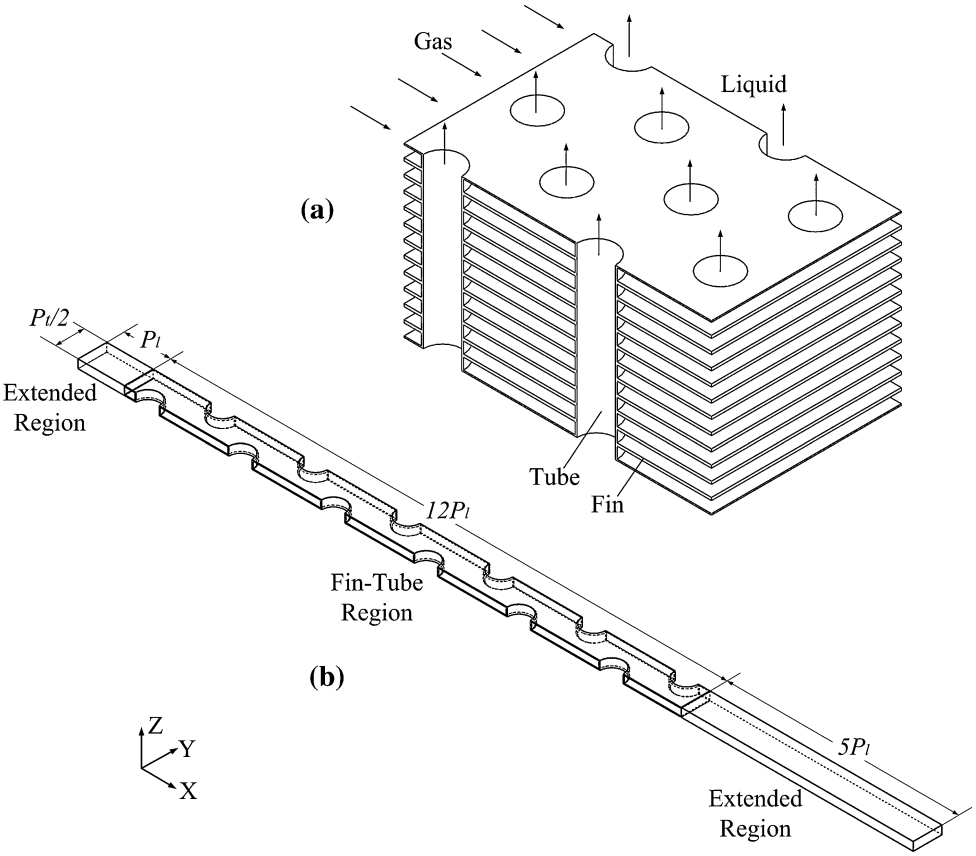

Fig. 1 A schematic diagram of a plain fin-and-tube heat exchanger and computational domain

is reflected in the following few aspects. First, local values or values for fully developed flow and heat transfer are the only two kinds of values that have a physical meaning when describing transport phenomena with VAT macro scale equations. Second, different experimental methods, assumptions or data reduction procedures are adopted by different researchers, and sometimes this information was not presented in the papers well due to the space limitation or some other reasons. Third, only part of the experimental data, which was enough to explain the phenomenon, was presented in these papers. At this time, CFD is an alternative approach for evaluating these closure terms [23–27]. It should be noted that if CFD is used to obtain the closure, the friction factor and heat transfer will be calculated more rigorously by integrating the complete closure formula over the REV.

In the following presentation, a plane fin-and-tube heat exchanger is first modeled based on Volume Averaging Theory. 3-D numerical calculations are made to simulate the heat transfer and fluid flow across the channels which consist of 6 REVs and the CFD discretization is validated by comparison with experiment. Then, the rigorously derived closure terms are evaluated over one of the selected REVs for a range of the design parameters, and correlations for friction factor and Nusselt number are developed for use with the simple equations.

2 VAT based modeling

A schematic diagram of a plane fin-and-tube heat exchanger is shown in Fig. 1a. Usually, there are three or more rows of tubes which are arranged in-line or staggered. Generally, liquid flows through the tubes and gas flows outside of the tubes. Because relatively large thermal resistance is encountered on the gas side, fins are employed to enlarge the heat transfer area and increase the heat transfer coefficient. This is a problem of conjugate heat transfer within a heterogeneous hierarchical structure. It is not easy to optimize this kind of problem since many parameters are required to describe the geometry. Simple equations are the only answer if one wants to find the optimum configuration for these kinds of conjugate heat transfer devices.

2.1 VAT based governing equations

Based on rigorous averaging techniques developed by Whitaker [15, 16] who focused on solving linear diffusion

problems and by Travkin and Catton [18, 20] who focused on solving nonlinear turbulent diffusion problems, the thermal physics and fluid mechanics governing equations in heterogeneous porous media were developed from the Navier–Stokes equation and the thermal energy equations. This is the starting point for studying flow and heat transfer in porous media and also the basis of the present work.

In this section, a model based on VAT is developed to describe transport phenomena in fin-and-tube heat exchangers. The air flow and water flow are considered to be 'porous flow', in which the term 'porous' is used in a broad sense.

The momentum equation for the air side is

$$-\frac{1}{\rho_1}\frac{\partial\langle\bar{p}_1\rangle_f}{\partial x}+\frac{\partial}{\partial z}\left(\langle m_1\rangle(\tilde{\nu}_{T_1}+\nu_1)\frac{\partial\tilde{\bar{u}}_1}{\partial z}\right)+f_1^*S_{w_1}\frac{\tilde{\bar{u}}_1^2}{2}=0 \tag{1}$$

and for the water side is

$$-\frac{1}{\rho_2}\frac{\partial\langle\bar{p}_2\rangle_f}{\partial z}+\frac{\partial}{\partial x}\left(\langle m_2\rangle(\tilde{\nu}_{T_2}+\nu_2)\frac{\partial\tilde{\bar{w}}_1}{\partial x}\right)+f_2^*S_{w_2}\frac{\tilde{\bar{w}}_2^2}{2}=0 \tag{2}$$

Because we are dealing with a conjugate type of problem, the thermal energy equations for both the solid and fluid states are required. For the air side, the VAT based energy equation is

$$\langle m_1\rangle\rho_1\tilde{\bar{u}}_1c_{p_1}\frac{\partial\tilde{\bar{T}}_1}{\partial x}=h_1^*S_{w_1}\left(\tilde{T}_s-\tilde{\bar{T}}_1\right) \tag{3}$$

and for the water side is

$$\langle m_2\rangle\rho_2\tilde{\bar{w}}_2c_{p_2}\frac{\partial\tilde{\bar{T}}_2}{\partial z}=h_2^*S_{w_2}\left(\tilde{T}_s-\tilde{\bar{T}}_2\right) \tag{4}$$

For the solid phase, the VAT based energy equation is

$$\begin{aligned}&\frac{\partial}{\partial x}\left[(1-\langle m_1\rangle-\langle m_2\rangle)k_s\frac{\partial\tilde{T}_s}{\partial x}\right]+\frac{\partial}{\partial z}\left[(1-\langle m_1\rangle-\langle m_2\rangle)k_s\frac{\partial\tilde{T}_s}{\partial z}\right]\\&=h_1^*S_{w_1}\left(\tilde{T}_s-\tilde{\bar{T}}_1\right)+h_2^*S_{w_2}\left(\tilde{T}_s-\tilde{\bar{T}}_2\right)\end{aligned} \tag{5}$$

here, $(1-\langle m_1\rangle-\langle m_2\rangle)$ can be considered as the averaged "blockage" (h_1 and h_2 were revised to h_1^* and h_2^* respectively in Eqs. 3–5).

2.2 Closure terms of the VAT equations

To complete the VAT based model, four closure terms need to be evaluated. It is believed that the only way to achieve substantial gains is to maintain the connection between porous media morphology and the rigorous formulation of mathematical equations for transport.

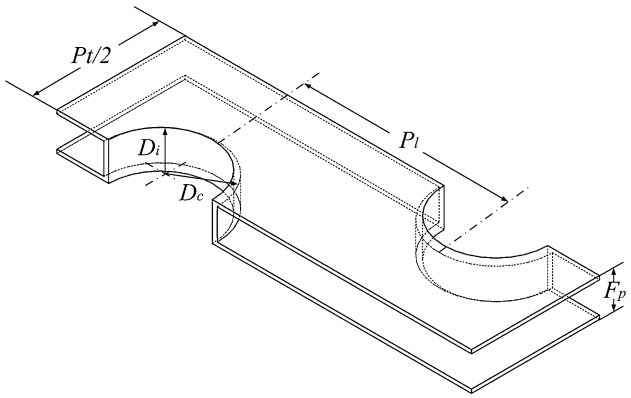

Fig. 2 Representative Elementary Volume (REV) for a fin-and-tube heat exchanger

Two of the closure terms, the averaged porosity and the specific surface area are geometrically defined and it is quite easy to determine them if one selects the REV correctly. The selection for a fin-and-tube heat exchanger, see Fig. 2 is seen to repeat in both the cross-stream and flow directions. The porosity for the air side of the fin-and-tube heat exchanger is

$$\langle m_1\rangle=\frac{\Delta\Omega_{f_1}}{\Delta\Omega}=1-\frac{\delta_f}{F_p}-\frac{\pi D_c^2\left(F_p-\delta_f\right)}{4P_lP_tF_p} \tag{6}$$

and for the water side is

$$\langle m_2\rangle=\frac{\Delta\Omega_{f_2}}{\Delta\Omega}=\frac{\pi D_i^2}{4P_lP_t} \tag{7}$$

The specific surface area for the air side is given by

$$S_{w_1}=\frac{A_{w_1}}{\Delta\Omega}=\frac{2P_lP_t-2\pi\left(\frac{D_c}{2}\right)^2+\pi D_c\left(F_p-\delta_f\right)}{P_lP_tF_p} \tag{8}$$

and for the water side is

$$S_{w_2}=\frac{A_{w_2}}{\Delta\Omega}=\frac{\pi D_i}{P_lP_t} \tag{9}$$

At this point, the VAT based model of FTHX is still not fully closed. The other two closure terms are the local friction factor, f^*, in the momentum equations and the local heat transfer coefficient, h^*, in the VAT energy equations and remain to be evaluated. To evaluate the closure terms, a commercial Finite Volume Method (FVM)-based code, CFX, was used to analyze the convective heat transfer in three-dimensional channels of fin-and-tube heat exchangers.

3 Numerical method and procedures

3.1 Computational domain and boundary conditions

The local closure values or closure values for fully developed flow and heat transfer are the only kinds of closure

Table 1 Boundary conditions

Inlet	$u = \text{const}$, $v = w = 0$, $T = \text{const}$
Outlet	$\frac{\partial u_i}{\partial x} = \frac{\partial T}{\partial x} = 0$
Eight surfaces of the extended region	Symmetric, slip and adiabatic wall
Interface between air and solid	No-slip, no thermal resistance
Tube inside wall	$u = v = w = 0$, $T_w = \text{const}$
The other surfaces	Symmetric

values that have physical meaning when describing transport phenomena with VAT based equations. For this reason, attention should be paid to the selection of physical model. The computational domain should be long enough, so that closure can be evaluated over an REV that is not affected by entrance or re-circulation effects near the outlet [28]. A computational domain with six REVs (twelve rows of tubes) was selected as the computational domain, see Fig. 1b.

The air velocity profile at the entrance is not uniform because of the fin thickness. The computational domain is extended upstream a distance of longitudinal tube pitch so that a uniform velocity distribution can be ensured at the domain inlet. The computational domain is extended downstream 5 times the longitudinal tube pitch, so that at the outer flow boundary no flow recirculation exits. The boundary conditions applied to the computational domain are tabulated in Table 1.

3.2 Grid system

The grid systems for all the FTHX models are built by Ansys Meshing. It is known that for flow-aligned geometries, hex mesh can provide higher-quality solutions with fewer cells than a comparable tet-mesh. Therefore, a structured hex-mesh, shown in Fig. 3, is carefully created, aligning the mesh with the flow to reduce false diffusion. In the fin and tube region, fine grid is built with prism layers being inserted in the near wall region, while in the extended parts, a coarser grid is adopted to conserve computational resources. A grid system with a gradual variation in and after the fin region is used to avoid the undesirable effect of an abrupt grid width change in the computing region.

Grid independence tests were made carefully by recursive refinement and comparison between the numerical simulation results. The above process was repeated until the variation of Nusselt number and friction factor was less than 0.5 %, so that the numerical predictions can be regarded as grid-independent. With the turbulence predictions employed, the meshes near the fluid solid interface are fine enough to resolve the flow behavior close to the no-slip wall. For all the simulation cases, y^+ values in the near-wall region are <1.

3.3 Mathematical model

In present CFD simulation, we consider the hot water flow through the tubes while the cooling air flows across the fin side. Due to the relatively large heat transfer coefficient on the tube side, the tube inner wall temperature was set equal to the fluid temperature. The conjugate effect of the tube wall was treated enabling the fin effect to be properly incorporated into the problem. The air flow is assumed to be three-dimensional, incompressible, steady state and turbulent. Buoyancy and radiation heat transfer effects are not taken into consideration. The three-dimensional governing equations for continuity, momentum and energy are as follows:

(1) Continuity equation

$$\frac{\partial \rho u_i}{\partial x_i} = 0 \tag{10}$$

(2) Momentum equation

$$\rho u_j \frac{\partial u_i}{\partial x_j} = \frac{\partial}{\partial x_j}\left[(\mu + \mu_T)\frac{\partial u_i}{\partial x_j}\right] - \frac{\partial p}{\partial x_i} \tag{11}$$

(3) Energy equation

$$\rho u_j \frac{\partial T}{\partial x_j} = \frac{\partial}{\partial x_j}\left[\left(\frac{\mu}{\mathrm{Pr}} + \frac{\mu_T}{\mathrm{Pr}_T}\right)\frac{\partial T}{\partial x_j}\right] \tag{12}$$

The k-ω based Shear-Stress-Transport (SST) model with automatic wall function treatment is used to predict the turbulent flow and heat transfer through the channel. The SST model blends the robust and accurate formulation of the k-ω model in the near-wall region with the free-stream independence of the k-ε model in the far field. The SST model gives a highly accurate prediction of the onset and the amount of flow separation under adverse pressure gradients by the inclusion of transport effects into the formulation of the eddy-viscosity. This results in a major improvement in terms of flow separation predictions [29]. The superior performance of the SST model has been demonstrated for high accuracy boundary layer simulations in a large number of validation studies.

Menter [30, 31] proposed the equations for the SST model as

$$\frac{D(\rho k)}{Dt} = \tilde{P}_k - \beta^* \rho k \omega + \frac{\partial}{\partial x_j}\left[(\mu + \sigma_k \mu_T)\frac{\partial k}{\partial x_i}\right] \tag{13}$$

$$\frac{D(\rho \omega)}{Dt} = \alpha \rho S^2 - \beta \rho \omega^2 + \frac{\partial}{\partial x_i}\left[(\mu + \sigma_\omega \mu_T)\frac{\partial \omega}{\partial x_i}\right] + 2(1 - F_1)\rho \sigma_{\omega_2}\frac{1}{\omega}\frac{\partial k}{\partial x_i}\frac{\partial \omega}{\partial x_i} \tag{14}$$

where the blending function F_1 is defined by:

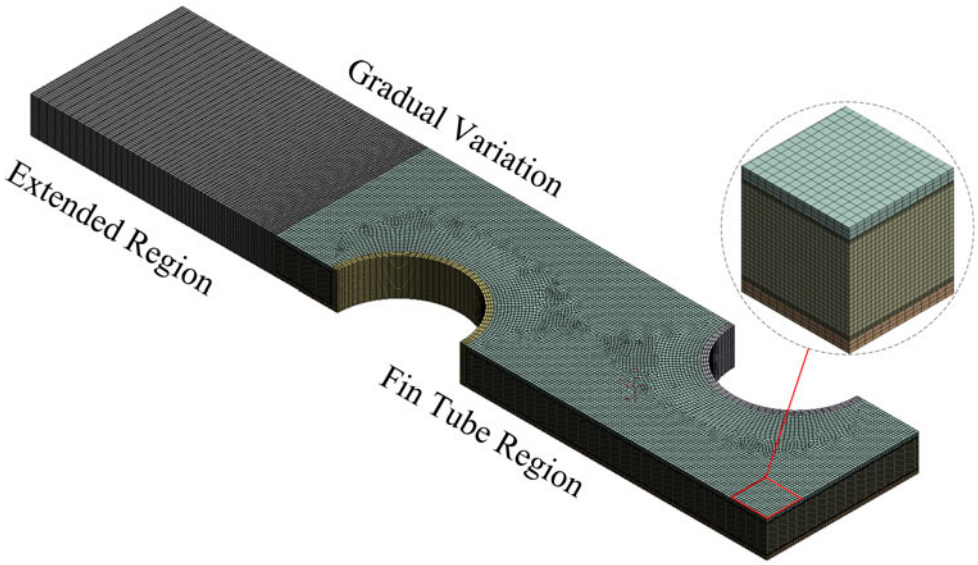

Fig. 3 Grid system of one fin-and-tube heat exchanger model

$$F_1 = \tanh\left\{\left\{\min\left[\max\left(\frac{\sqrt{k}}{\beta^*\omega y}, \frac{500v}{y^2\omega}\right), \frac{4\rho\sigma_{\omega_2}k}{CD_{k\omega}y^2}\right]\right\}^4\right\} \tag{15}$$

in which

$$CD_{k\omega} = \max\left(2\rho\sigma_{\omega_2}\frac{1}{\omega}\frac{\partial k}{\partial x_j}\frac{\partial \omega}{\partial x_j}, 10^{-10}\right) \tag{16}$$

The turbulent eddy viscosity is computed from:

$$v_T = \frac{a_1 k}{\max(a_1\omega, SF_2)} \tag{17}$$

where S is the invariant measure of the strain rate and F_2 is a second blending function defined by

$$F_2 = \tanh\left\{\left[\max\left(2\frac{\sqrt{k}}{\beta^*\omega y}, \frac{500v}{y^2\omega}\right)\right]^2\right\} \tag{18}$$

To prevent the build-up of turbulence in stagnation regions, a production limiter is used in the SST model:

$$P_k = \mu_t\frac{\partial u_i}{\partial x_j}\left(\frac{\partial u_i}{\partial x_j} + \frac{\partial u_j}{\partial x_i}\right) \rightarrow \tilde{P}_k = \min(P_k, 10\cdot\beta^*\rho k\omega) \tag{19}$$

Each of the constants is a blend of the corresponding constants of the k-ε and the k-ω model:

$$\varphi = F_1\varphi_1 + (1 - F_1)\varphi_2 \tag{20}$$

The constants for this model take the following values

$$\begin{aligned} &\beta^* = 0.09, \\ &\alpha_1 = 5/9,\ \beta_1 = 3/40,\ \sigma_{k1} = 0.85,\ \sigma_{\omega 1} = 0.5, \\ &\alpha_2 = 0.44,\ \beta_2 = 0.0828,\ \sigma_{k2} = 1,\ \sigma_{\omega 2} = 0.856. \end{aligned} \tag{21}$$

The CFD code solves the Reynolds-averaged Navier–Stokes equations with a high resolution scheme for the advection terms as well as turbulence numerics. The fully coupled momentum and energy equations are solved simultaneously. The RMS type residual for solution convergence criteria is set to be 10^{-5} for the momentum balance and 10^{-6} for the energy equation.

4 Closure evaluation

Closure evaluation described in this section consists of three parts. First, the two different length scales used to evaluate the flow and heat transfer characteristics of the scale-roughened channels are defined. Second, the computational model and the method adopted in current numerical simulations are verified and validated by comparing the CFD results with experimental data. Third, two correlations which serve as closure for the VAT based model are developed based on the simulation results.

4.1 Length scales

Before evaluating the closure terms, it is interesting to note that using a particular length scale leads to a parameter that is very beneficial when evaluating the heat transfer coefficient and friction factor. It was shown by Travkin and Catton [20] that globular media morphologies can be

described in terms of S_w, $\langle m \rangle$ and d_p and can generally be considered to be spherical particles with

$$S_w = \frac{6(1-\langle m \rangle)}{d_p} \tag{22}$$

$$D_h = \frac{2}{3}\frac{\langle m \rangle}{(1-\langle m \rangle)} d_p \tag{23}$$

This expression has the same dependency on equivalent pore diameter as found for a one diameter capillary morphology leading naturally to

$$S_w = \frac{6(1-\langle m \rangle)}{d_p} = \frac{6(1-\langle m \rangle)}{\frac{3}{2}\frac{(1-\langle m \rangle)}{\langle m \rangle} D_h} = \frac{4\langle m \rangle}{D_h} \tag{24}$$

This observation leads to defining a simple "universal" porous media length scale

$$D_h = \frac{4\langle m \rangle}{S_w} \tag{25}$$

that meets the needs of both morphologies: capillary and globular. This was also recognized by Whitaker [16] when he used a very similar (differing by a constant) length scale to correlate heat transfer for a wide variety of morphologies. Zhou et al. [21] also showed that using the 'porous media' length scale is very beneficial in collapsing complex data yielding simple heat transfer and friction factor correlations. For the present fin-and-tube heat exchangers, the hydraulic diameter of the air side is defined as

$$D_{h_1} = \frac{4\langle m_1 \rangle}{S_{w_1}} = \frac{\left(4P_l P_t - \pi D_c^2\right)\left(F_p - \delta_f\right)}{2P_l P_t - 2\pi\left(\frac{D_c}{2}\right)^2 + \pi D_c\left(F_p - \delta_f\right)} \tag{26}$$

The hydraulic diameter of the water side is defined as

$$D_{h_2} = \frac{4 \cdot \langle m_2 \rangle}{S_{w_2}} = \frac{4 \cdot \frac{\pi D_i^2}{4P_l P_t}}{\frac{\pi D_i}{P_l P_t}} = D_i \tag{27}$$

The Reynolds number defined using the VAT suggested length scale is

$$\mathrm{Re}_{D_h} = \frac{\rho \tilde{\bar{u}} D_h}{\mu} \tag{28}$$

To validate the CFD simulation results, the Reynolds number is defined the same as that used by Tang et al. [10]

$$\mathrm{Re}_{D_c} = \frac{\rho u_{\max} D_c}{\mu}. \tag{29}$$

4.2 Validation and verification

To verify the computational model and the method adopted in numerical simulation, preliminary computations were first conducted for a FTHX which had the same dimensions as the one experimentally tested by Tang et al. [10].

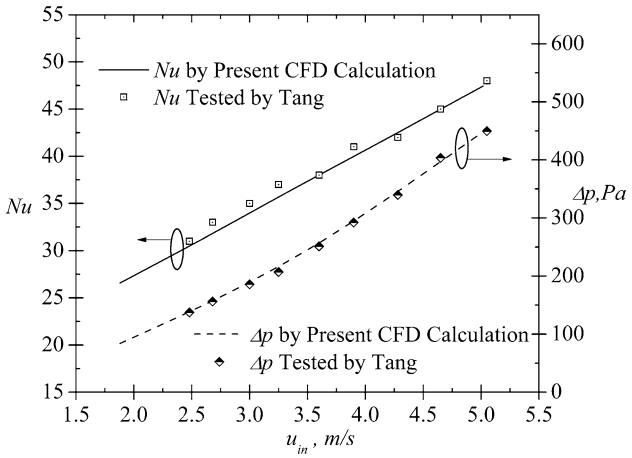

Fig. 4 Comparison between the present CFD results and experimental data by Tang et al. [10]

Definitions for the characteristic quantities which are used in the validation and verification are presented the following:

$$Nu = \frac{hD_c}{k_f} \tag{30}$$

$$h = \frac{\dot{m} c_p (T_{\mathrm{in}} - T_{\mathrm{out}})}{A_o \Delta T \eta_o} \tag{31}$$

$$\Delta T = \frac{\max(T_{\mathrm{in}} - T_w, T_{\mathrm{out}} - T_w) - \min(T_{\mathrm{in}} - T_w, T_{\mathrm{out}} - T_w)}{\log[\max(T_{\mathrm{in}} - T_w, T_{\mathrm{out}} - T_w)/\min(T_{\mathrm{in}} - T_w, T_{\mathrm{out}} - T_w)]} \tag{32}$$

$$\eta_o = 1 - \frac{A_f}{A_o}\left(1 - \eta_f\right) \tag{33}$$

$$\eta_f = \frac{\tanh(mr\phi)}{mr\phi} \tag{34}$$

where

$$m = \sqrt{\frac{2h}{k_f \delta_f}} \tag{35}$$

$$\phi = \left(\frac{R_{eq}}{r} - 1\right)\left[1 + 0.35\ln\left(\frac{R_{eq}}{r}\right)\right] \tag{36}$$

$$\frac{R_{eq}}{r} = 1.27\frac{X_M}{r}\left(\frac{X_L}{X_M} - 0.3\right)^{1/2} \tag{37}$$

$$X_L = \frac{\sqrt{(P_t/2)^2 + P_l^2}}{2} \tag{38}$$

$$X_M = P_t/2 \tag{39}$$

$$f = \frac{\Delta p}{\frac{1}{2}\rho u_{\max}^2} \cdot \frac{D_c}{L} \tag{40}$$

From Fig. 4 it is seen that the maximum deviation of Nusselt number and friction factor from experiment are 4.8 and 2 % with the average deviation being around 3.5 and 1 % respectively. Our predicted results and the experimental data agree very well, thereby showing the reliability of the physical model and the adopted numerical method.

4.3 Closure

Travkin and Catton [20] rigorously derive the closure terms for VAT based model from the lower scale governing equations. The closure term in the VAT momentum equation, f^*, has the form

$$f^* = 2\frac{\int_{\partial S_w}\bar{p}\cdot d\vec{s}}{\rho_f\tilde{\bar{u}}^2 A_{wp}}\frac{S_{wp}}{S_w} + 2\frac{\int_{\partial S_w}\tau_{wL}\cdot d\vec{s}}{\rho_f\tilde{\bar{u}}^2 A_w} + 2\frac{\int_{\partial S_w}\tau_{wT}\cdot d\vec{s}}{\rho_f\tilde{\bar{u}}^2 A_w} - \frac{\frac{\partial}{\partial x_j}\langle\hat{\bar{u}}_i\hat{\bar{u}}_j\rangle_f}{\frac{1}{2}\rho\tilde{\bar{u}}^2} + \frac{\frac{\partial}{\partial x_j}\left(\left\langle\tilde{v}_T\frac{\partial\tilde{\bar{u}}_i}{\partial x_j}\right\rangle_f\right)}{\frac{1}{2}\rho\tilde{\bar{u}}^2} \quad (41)$$

The first three terms are form drag, and laminar and turbulent contributions to skin friction, respectively. The fourth term represents the spatial flow oscillations, which are a function of porous media morphology and tell one how flow deviates from some mean value over the REV. The fifth term represents flow oscillations that are due to Reynolds stresses and are a function of porous media morphology and its time averaged flow oscillations.

The closure terms in the VAT energy equation, h^*, can be defined in various ways and in general will depend on how many of the integrals appearing in the VAT equation one uses and lumps into a single transport coefficient, see Travkin and Catton [20]. The nature of the equation shows that the energy transferred from the surface is integrated over an area and then divided by the chosen REV volume; therefore, the heat transfer coefficient is defined in terms of porous media morphology, usually described by specific surface and porosity.

The complete form of the closure term h^* is

$$h^* = \frac{\frac{1}{\Delta\Omega}\int_{\partial S_w}(k_f + k_T)\nabla T_f\cdot dS}{S_w(\tilde{T}_s - \tilde{T}_f)} - \frac{\rho_f c_{pf}\nabla\cdot\left(\langle m\rangle\widetilde{\hat{u}_f\hat{T}_f}\right)}{S_w(\tilde{T}_s - \tilde{T}_f)} + \frac{\nabla\cdot\left(\frac{k_f}{\Delta\Omega}\int_{\partial S_w}T_f dS\right)}{S_w(\tilde{T}_s - \tilde{T}_f)} \quad (42)$$

In most engineered devices, the geometry is regular and a well-chosen REV will lead to only the first term being needed. The second term is identically zero for regular repeating geometries and the third is Biot number dependent. However, when in doubt, one should use the complete form given by Eq. (42).

After solving the three-dimensional governing Eqs. (10–12) with appropriate boundary conditions, the closure for the VAT based momentum equation and energy equation is obtained by integrating Eqs. (41) and (42) over one of the six REVs selected from the fully developed region to compute the friction factor and heat transfer coefficient. The readers can refer to the former work by the authors [28] to see how to select a correct REV to do the closure evaluation.

To demonstrate the value of the VAT based length scale, 6 more different sets of design dimensions besides the one which is the same as what Tang et al. [10] experimentally tested, see Table 2, were simulated at different Re_{D_c}, ranging from 2,000 to 12,000.

The Nusselt number and friction factor evaluated using the length scale D_c as a function of Re_{D_c} for fin-and-tube heat exchangers with different dimensions are shown in Figs. 5 and 6. The numerically predicted results are scattered, leading to seven different $Nu_{D_c} - \mathrm{Re}_{D_c}$ and $f_{D_c} - \mathrm{Re}_{D_c}$ curves. However, the Nusselt number and friction factor obtained by evaluating the rigorously derived closure terms, Eqs. (41) and (42), collapse to two single curves, shown in Figs. 7 and 8.

Travkin and Catton [17] and Zhou et al. [21] showed that using the VAT suggested length scale, enables one to write the friction factor of porous media in the following form:

$$f^* = \frac{A}{\mathrm{Re}_{D_h}} + B \quad (43)$$

The constants A and B correspond to different types of morphologies of porous media, with A = 100/3 and B = 7/12 for the Ergun equation for packed bed porous media, A = 50 and B = 0.145 for the pin fin array [26].

With the help of JMP 9, an available statistical analysis tool, the collapsed data enabled us to develop a simple correlation of friction factor for the air side,

$$f_{D_h} = \frac{128.2}{\mathrm{Re}_{D_h}} + 0.149 \quad (44)$$

A comparison of values of A and B with other morphologies is shown in Table 3.

Similarly, the collapsed Nusselt number was correlated as

$$Nu_{D_h} = 0.171\mathrm{Re}_{D_h}^{0.559}\mathrm{Pr}^{1/3} \quad (45)$$

Figures 9 and 10 show the comparison between the numerical simulation results and the results predicted by the proposed correlations. The proposed friction factor correlation, Eq. (44), can predict 83.3 % of data within a deviation of 10 % and an average deviation of 2.6 %. The correlation of Nusselt number, Eq. (45), can describe all the simulation results within a deviation of 10 % and an average deviation of 1.6 %.

It should be noted that the correlations proposed by Zhou et al. [21] was obtained by rescaling experimental

Table 2 Geometric dimensions of the numerically tested fin-and-tube heat exchangers

	P_t/D_c	P_l/D_c	F_p/D_c
Base case	2.26	1.83	0.167
Case 1	2.53	2.05	0.187
Case 2	2.04	1.65	0.150
Case 3	2.26	1.72	0.167
Case 4	2.26	1.94	0.167
Case 5	2.04	1.83	0.167
Case 6	2.47	1.83	0.167

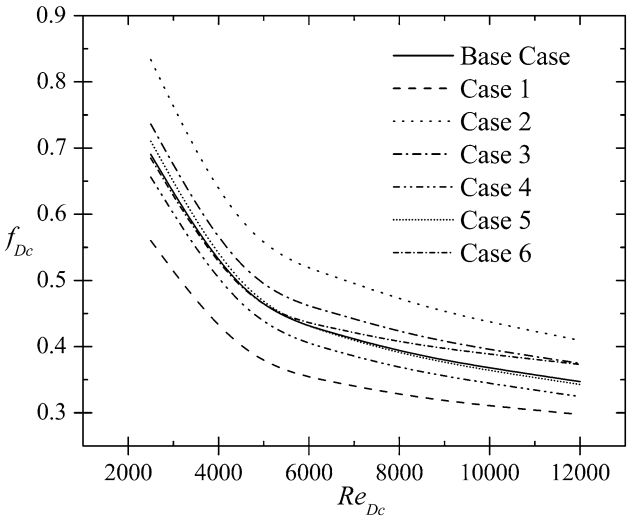

Fig. 5 Friction factor as a function of Re_{D_c} using D_c as the length scale

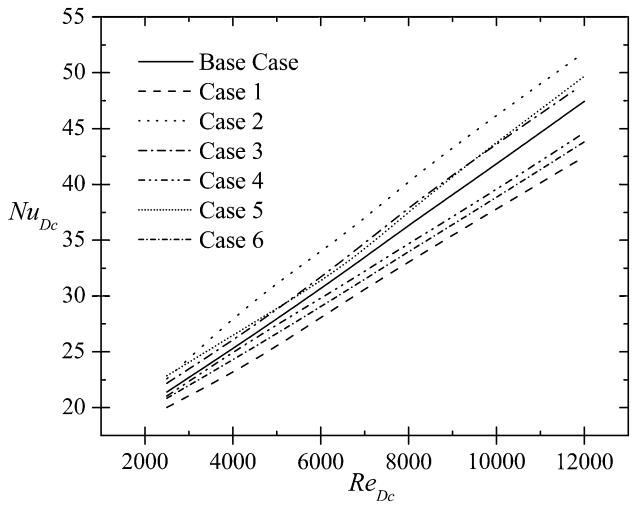

Fig. 6 Nusselt number as a function of Re_{D_c} using D_c as the length scale

data available in public literature which were average values, while the correlations proposed in the present paper were obtained by evaluating the rigorously derived closure

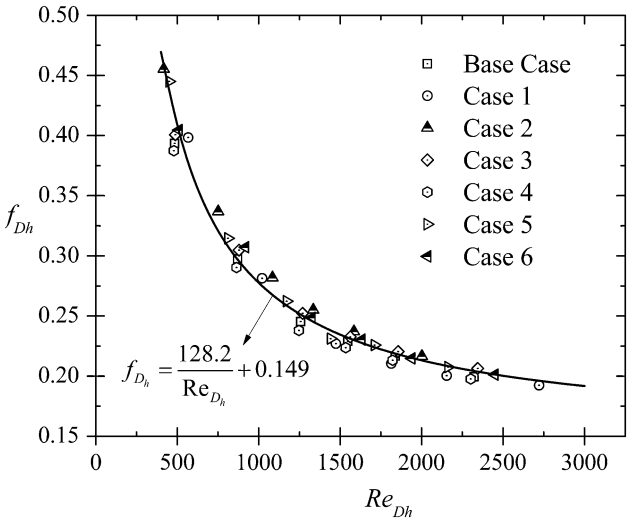

Fig. 7 Friction factor as a function of Re_{D_h} using D_h as the length scale

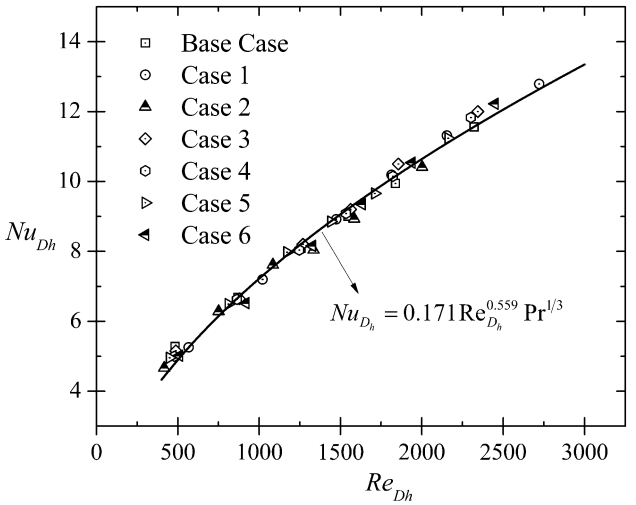

Fig. 8 Nusselt number as a function of Re_{D_h} using D_h as the length scale

terms over a selected REV which were local values. The comparison of the two different sets of correlations is shown in Fig. 11. It should be pointed out that these correlations are not necessarily the most accurate available, however, they have wide application, are easy to use, and are quite satisfactory for most design calculations [16]. Also, for optimization, extreme accuracy is not vital because variation in the parameter being optimized can be as much as an order of magnitude.

For closure of the water side, the friction factor and Nusselt number correlations for fully developed flow in a pipe are applicable to close the water side VAT equations

Table 3 Closure coefficients of friction factor for different morphologies

Morphology	A	B	Porosity range
Packed bed	100/3	7/12	0.3–0.72
Pin fins-inline	50	0.145	0.65–0.91
Pin fins-staggered	50	0.145	0.65–0.91
Staggered plain fin-and-tube HX (average)	112.4	0.252	0.65–0.9
Staggered plain fin-and-tube HX (local)	128.2	0.149	0.65–0.9

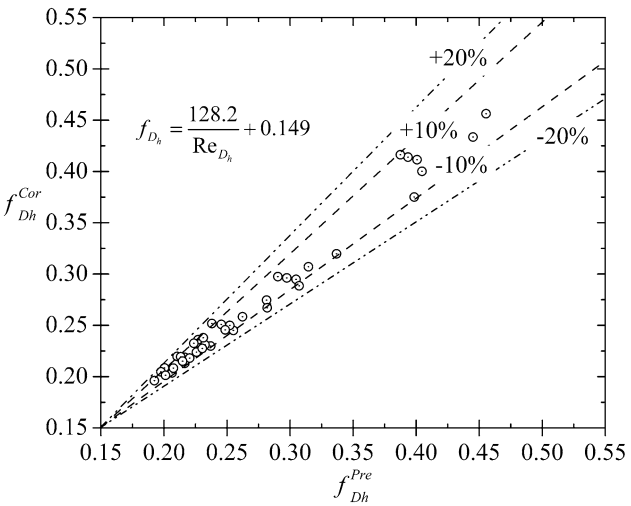

Fig. 9 Deviation of the proposed friction factor correlation

since $D_{h_2} = D_i$. Petukhov correlated the friction factor for turbulent pipe flow as follows

$$f_2^* = (0.790 \ln \mathrm{Re}_{D_h} - 1.64)^{-2} \tag{46}$$

As for the heat transfer coefficient, h_2^*, Whitaker showed that the experimental data of Nusselt number from a number of investigators for turbulent pipe flow is quite nicely re-correlated by the expression

$$Nu_2^* = 0.015 \mathrm{Re}_{D_h}^{0.83} \mathrm{Pr}^{0.42} \left(\frac{\mu_b}{\mu_0}\right)^{0.14} = \frac{h_2^* D_{h_2}}{k_{f2}} \tag{47}$$

At this point, the VAT based model of FTHXs is fully closed. With the closure correlations, the governing equation set is relatively simple and can be solved discretely in seconds. With the help of a statistical tool for Design of Experiments (DOE) or Genetic Algorithm (GA), a FTHX could be designed and optimized in an hour, instead of days of CFD or experimental work. How to design and optimize a FTHX based on VAT will be presented in a future paper.

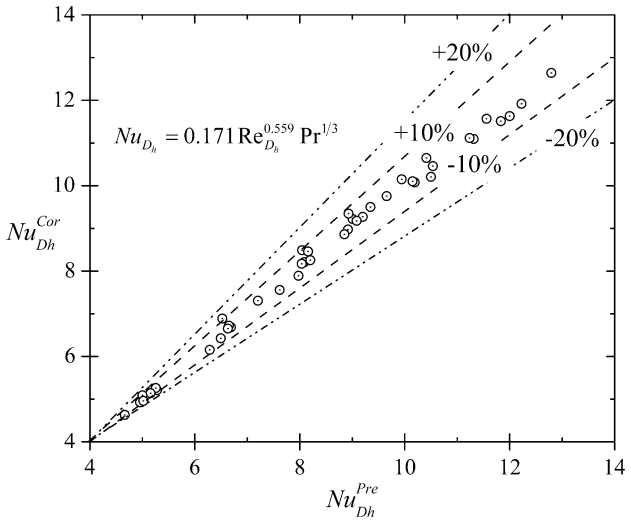

Fig. 10 Deviation of the proposed Nusselt number correlation

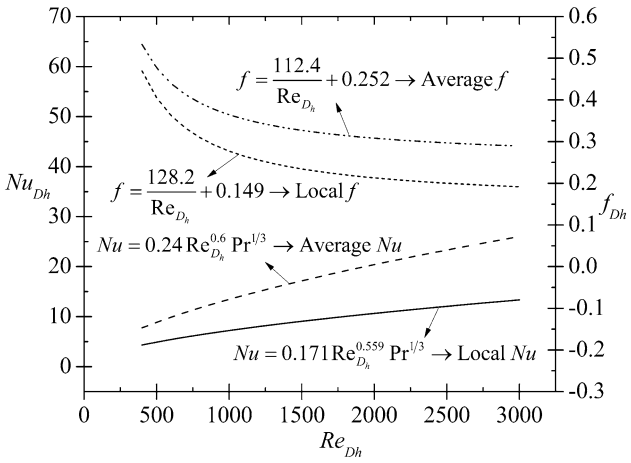

Fig. 11 Local and average closure

5 Concluding remarks

Volume Averaging Theory is little more than a judicious application of Green's and Stokes' theorems to carry out the integration needed to average the point-wise conservation equations in a rigorous way. By treating the closure part of the problem carefully, the result remains rigorous in spite of its simplicity. Many everyday engineered devices are hierarchical and heterogeneous and can be effectively treated by application of VAT. It is an approach that can be applied to many different types of transport phenomena, see Travkin and Catton [20].

The present paper describes an effort to develop a VAT based hierarchical model for a plane fin-and-tube heat exchanger and obtain the closure for the model by CFD code. A length of 6 REVs was selected to be the

computational domain. The rigorously derived closure terms of heat transfer coefficient and friction factor were evaluated over the carefully selected REV. Two correlations of friction factor and Nusselt number were established based on the simulation results.

With closure of the friction factor and the heat transfer coefficient, the problem is closed and the porous media governing equations derived from VAT are

$$\tilde{M}(\langle m \rangle, S_w, f^*) \tag{48}$$

$$\tilde{T}_s(\langle m \rangle, S_w, h^*) \tag{49}$$

$$\tilde{T}_f(\langle m \rangle, S_w, h^*) \tag{50}$$

where $\tilde{M}$ stands for averaged momentum equation variables, $\tilde{T}_s$ and $\tilde{T}_f$ stand for averaged energy equation variables for solid and fluid phase. The macro scale equations are functions only of porous media morphology, represented by porosity and specific surface area, and its closure.

Acknowledgments The support of a DARPA initiated grant within the MACE program, Grant No. W31P4Q-09-1-0005, is gratefully acknowledged. The views, opinions, and/or findings contained in this article are those of the author and should not be interpreted as representing the official views or policies, either expressed or implied, of the Defense Advanced Research Projects Agency or the Department of Defense.

References

1. Rich DG (1973) The effect of fin spacing on the heat transfer and friction performance of multirow, smooth plate fin-and-tube heat exchangers. ASHRAE Trans 79:135–145
2. Rich DG (1975) The effect of the number of tubes rows on heat transfer performance of smooth plate fin-and-tube heat exchangers. ASHRAE Trans 81:307–317
3. McQuiston FC (1978) Heat mass and momentum transfer data for five plate-fin-tube heat transfer surfaces. ASHRAE Trans Part 1:266–293
4. McQuiston FC (1978) Correlations of heat mass and momentum transport coefficients for plate-fin-tube heat transfer surfaces with staggered tubes. ASHRAE Trans Part 1:294–308
5. Wang C–C, Chang Y-J, Hsieh Y-C, Lin Y-T (1996) Sensible heat and friction characteristics of plate fin-and-tube heat exchangers having plane fins. Int J Refrig 19:223–230
6. Wang C–C, Chi K-Y (2000) Heat transfer and friction characteristics of plain fin-and-tube heat exchangers, part I: new experimental data. Int J Heat Mass Transf 43:2681–2691
7. Wang C–C, Chi K-Y, Chang C-J (2000) Heat transfer and friction characteristics of plain fin-and-tube heat exchangers, part II: correlation. Int J Heat Mass Transf 43:2693–2700
8. Tang L-H, Min Z, Xie G-N, Wang Q-W (2009) Fin pattern effects on air-side heat transfer and friction characteristics of fin-and-tube heat exchangers with large number of large-diameter tube rows. Heat Transf Eng 30:171–180
9. Jang J-Y, Chen L-K (1997) Numerical analysis of heat transfer and fluid flow in a three-dimensional wavy-fin and tube heat exchanger. Int J Heat Mass Transf 40:3981–3990
10. Tang LH, Zeng M, Wang QW (2009) Experimental and numerical investigation on air-side performance of fin-and-tube heat exchangers with various fin patterns. Exp Therm Fluid Sci 33:818–827
11. Xie G, Wang Q, Sunden B (2009) Parametric study and multiple correlations on air-side heat transfer and friction characteristics of fin-and-tube heat exchangers with large number of large-diameter tube rows. Appl Therm Eng 29:1–16
12. Lu C-W, Huang J-M, Nien WC, Wang C–C (2011) A numerical investigation of the geometric effects on the performance of plate finned-tube heat exchanger. Energy Convers Manage 52:1638–1643. doi:10.1016/j.enconman.2010.10.026
13. Anderson TB, Jackson R (1967) Fluid mechanical description of fluidized beds. Equations of motion. Ind Eng Chem Fundam 6:527–539. doi:10.1021/i160024a007
14. Gaitonde NY, Middleman S (1967) Flow of viscoelastic fluids through porous media. Ind Eng Chem Fundam 6:145–147. doi:10.1021/i160021a026
15. Whitaker S (1967) Diffusion and dispersion in porous media. AIChE J 13:420–427
16. Whitaker S (1972) Forced convection heat transfer correlations for flow in pipes, past flat plates, single cylinders, single spheres, and for flow in packed beds and tube bundles. AIChE J 18:361–371
17. Travkin V, Catton I (1995) A two-temperature model for turbulent flow and heat transfer in a porous layer. J Fluids Eng 117:181–188
18. Travkin VS, Catton I (1998) Porous media transport descriptions—non-local, linear and non-linear against effective thermal/fluid properties. Adv Colloid Interface Sci 76–77:389–443
19. Travkin VS, Catton I (1999) Turbulent flow and heat transfer modeling in a flat channel with regular highly rough walls. Int J Fluid Mech Res 26:159–199
20. Travkin VS, Catton I (2001) Transport phenomena in heterogeneous media based on volume averaging theory. Adv Heat Transf 34:1–144
21. Zhou F, Hansen NE, Geb DJ, Catton I (2011) Obtaining closure for fin-and-tube heat exchanger modeling based on volume averaging theory (VAT). J Heat Transf 133:111802
22. Geb D, Zhou F, Catton I (2012) Internal heat transfer coefficient determination in a packed bed from the transient response due to solid phase induction heating. J Heat Transf 134:042604
23. Horvat A, Catton I (2003) Numerical technique for modeling conjugate heat transfer in an electronic device heat sink. Int J Heat Mass Transf 46:2155–2168
24. Horvat A, Catton I (2003) Application of Galerkin method to conjugate heat transfer calculation. Numer Heat Transf Part B Fundam Int J Comput Methodol 44:509–531
25. Horvat A, Mavko B (2005) Hierarchic modeling of heat transfer processes in heat exchangers. Int J Heat Mass Transf 48:361–371
26. Horvat A, Mavko B (2005) Calculation of conjugate heat transfer problem with volumetric heat generation using the Galerkin method. Appl Math Model 29:477–495
27. Vadnjal A (2009) Modeling of a heat sink and high heat flux vapor chamber. PhD Thesis, Aerospace Engineering University of California Los Angeles, Los Angeles, p 209
28. Zhou F, Hansen NE, Geb DJ, Catton I (2011) Determination of the number of tube rows to obtain closure for volume averaging theory based model of fin-and-tube heat exchangers. J Heat Transf 133:121801
29. Zhou F, Catton I (2011) Numerical evaluation of flow and heat transfer in plate-pin fin heat sinks with various pin cross-sections. Numer Heat Transf Part A Appl 60:107–128
30. Menter FR (1994) Two-equation eddy-viscosity turbulence models for engineering applications. AIAA J 32:1598–1605
31. Menter FR, Kuntz M, Langtry R (2003) Ten years of industrial experience with the SST turbulence model. Turbul Heat Mass Transf 4:625–632